

# InGaAs/AlGaAsSb avalanche photodiode with high gain-bandwidth product

SHIYU XIE,<sup>1,3</sup> XINXIN ZHOU,<sup>1</sup> SHIYONG ZHANG,<sup>1</sup> DAVID J. THOMSON,<sup>2</sup> XIA CHEN,<sup>2</sup> GRAHAM T. REED,<sup>2</sup> JO SHIEN NG,<sup>1</sup> AND CHEE HING TAN<sup>1,\*</sup>

<sup>1</sup>Department of Electronic and Electrical Engineering, University of Sheffield, Sheffield S3 7HQ, UK

<sup>2</sup>Optoelectronics Research Centre, University of Southampton, Highfield, Southampton SO17 1BJ, UK

<sup>3</sup>Present address: School of Physics and Astronomy, Cardiff University, Queen's Building, The Parade, Cardiff CF24 3AA, UK

\*c.h.tan@sheffield.ac.uk

**Abstract:** Increasing reliance on the Internet places greater and greater demands for high-speed optical communication systems. Increasing their data transfer rate allows more data to be transferred over existing links. With optical receivers being essential to all optical links, bandwidth performance of key components in receivers, such as avalanche photodiodes (APDs), must be improved. The APDs rely on In<sub>0.53</sub>Ga<sub>0.47</sub>As (grown lattice-matched to InP substrates) to efficiently absorb and detect the optical signals with 1310 or 1550 nm wavelength, the optimal wavelengths of operation for these optical links. Thus developing InP-compatible APDs with high gain-bandwidth product (GBP) is important to the overall effort of increasing optical links' data transfer rate. Here we demonstrate a novel InGaAs/AlGaAsSb APD, grown on an InP substrate, with a GBP of 424 GHz, the highest value reported for InP-compatible APDs, which is clearly applicable to future optical communication systems at or above 10 Gb/s. The data reported in this article are available from the figshare digital repository (<https://dx.doi.org/10.15131/shef.data.3827460.v1>).

Published by The Optical Society under the terms of the [Creative Commons Attribution 4.0 License](#). Further distribution of this work must maintain attribution to the author(s) and the published article's title, journal citation, and DOI.

**OCIS codes:** (040.1345) Avalanche photodiodes (APDs); (060.2330) Fiber optics communications.

## References and links

1. High throughput Computing Data Center Architecture, Huawei Technologies Co., Ltd., Shenzhen, China, (2014).
2. R. B. Emmons, "Avalanche-Photodiode Frequency Response," *J. Appl. Phys.* **38**(9), 3705 (1967).
3. D. S. G. Ong, M. M. Hayat, J. P. R. David, and J. S. Ng, "Sensitivity of High-Speed Lightwave System Receivers Using InAlAs Avalanche Photodiodes," *IEEE Photonics Technol. Lett.* **23**(4), 233–235 (2011).
4. J. C. Campbell, W. T. Tsang, G. J. Qua, and B. C. Johnson, "High-speed InP/InGaAsP/InGaAs avalanche photodiodes grown by chemical beam epitaxy," *IEEE J. Quantum Electron.* **24**(3), 496–500 (1988).
5. L. E. Tarof, J. Yu, R. Bruce, D. G. Knight, T. Baird, and B. Oosterbrink, "High-frequency performance of separate absorption grading, charge, and multiplication InP/InGaAs avalanche photodiodes," *IEEE Photonics Technol. Lett.* **5**(6), 672–674 (1993).
6. A.-W. Yue, R.-F. Wang, B. Xiong, and J. Shi, "Fabrication of a 10 Gb/s InGaAs/InP Avalanche Photodiode with an AlGaInAs/InP Distributed Bragg Reflector," *Chin. Phys. Lett.* **30**(3), 038501 (2013).
7. T. Nakata, T. Takeuchi, I. Watanabe, K. Makita, and T. Torikai, "10 Gbit/s high sensitivity, low-voltage-operation avalanche photodiodes with thin InAlAs multiplication layer and waveguide structure," *Electron. Lett.* **36**(24), 2033–2034 (2000).
8. A. Rouvie, D. Carpentier, N. Lagay, J. Decobert, F. Pommereau, and M. Achouche, "High Gain × Bandwidth Product Over 140-GHz Planar Junction AllInAs Avalanche Photodiodes," *IEEE Photonics Technol. Lett.* **20**(6), 455–457 (2008).
9. S. Xie, S. Zhang, and C. H. Tan, "InGaAs/InAlAs avalanche photodiode with low dark current for high-speed operation," *IEEE Photonics Technol. Lett.* **27**(16), 1745–1748 (2015).
10. I. Watanabe, M. Tsuji, M. Hayashi, K. Makita, and K. Taguchi, "Design and performance of InAlGaAs/InAlAs superlattice avalanche photodiode," *J. Lightwave Technol.* **15**(6), 1012–1019 (1997).
11. M. Nada, Y. Muramoto, H. Yokoyama, T. Ishibashi, and S. Kodama, "InAlAs APD with high multiplied responsivity-bandwidth product (MR-bandwidth product) of 168 A/W. GHz for 25 Gbit/s high-speed operations," *Electron. Lett.* **48**(7), 397–399 (2012).

12. M. Ren, S. J. Maddox, M. E. Woodson, Y. Chen, S. R. Bank, and J. C. Campbell, "AlInAsSb separate absorption, charge, and multiplication avalanche photodiodes," *Appl. Phys. Lett.* **108**(19), 191108 (2016).
13. A. R. J. Marshall, P. J. Ker, A. Krysa, J. P. R. David, and C. H. Tan, "High speed InAs electron avalanche photodiodes overcome the conventional gain-bandwidth product limit," *Opt. Express* **19**(23), 23341–23349 (2011).
14. Y. Kang, H.-D. Liu, M. Morse, M. J. Paniccia, M. Zadka, S. Litski, G. Sarid, A. Pauchard, Y.-H. Kuo, H.-W. Chen, W. S. Zaoui, J. E. Bowers, A. Beling, D. C. McIntosh, X. Zheng, and J. C. Campbell, "Monolithic germanium/silicon avalanche photodiodes with 340 GHz gain–bandwidth product," *Nat. Photonics* **3**(1), 59–63 (2009).
15. N. Duan, T.-Y. Liow, A. E.-J. Lim, L. Ding, and G. Q. Lo, "310 GHz gain-bandwidth product Ge/Si avalanche photodetector for 1550 nm light detection," *Opt. Express* **20**(10), 11031–11036 (2012).
16. L. Virost, P. Crozat, J.-M. Fédéli, J.-M. Hartmann, D. Marris-Morini, E. Cassan, F. Boeuf, and L. Vivien, "Germanium avalanche receiver for low power interconnects," *Nat. Commun.* **5**, 4957 (2014).
17. J. Xie, S. Xie, R. C. Tozer, and C. H. Tan, "Excess noise characteristics of thin AlAsSb APDs," *IEEE Trans. Electron Dev.* **59**(5), 1475–1479 (2012).
18. S. Xie and C. H. Tan, "AlAsSb avalanche photodiodes with a sub-mV/K temperature coefficient of breakdown voltage," *IEEE J. Quantum Electron.* **47**(11), 1391–1395 (2011).
19. X. Zhou, S. Zhang, J. P. R. David, J. S. Ng, and C. H. Tan, "Avalanche breakdown characteristics of  $\text{Al}_{1-x}\text{Ga}_x\text{As}_{0.56}\text{Sb}_{0.44}$  quaternary alloys," *IEEE Photonics Technol. Lett.* (to be published).
20. Z. Hang, H. Shen, and F. H. Pollak, "Temperature dependence of the  $E_g$  and  $\Delta_g$  gaps of InP up to 600 °C," *Solid-St. Commun.* **73**, 15–18 (1990).
21. D. K. Gaskill, N. Bottka, L. Aina, and M. Mattingly, "Band-gap determination by photoreflectance of InGaAs and InAlAs lattice matched to InP," *Appl. Phys. Lett.* **56**(13), 1269 (1990).
22. L. J. J. Tan, D. S. G. Ong, J. S. Ng, C. H. Tan, S. K. Jones, Y. Qian, and J. P. R. David, "Temperature Dependence of Avalanche Breakdown in InP and InAlAs," *IEEE J. Quantum Electron.* **46**(8), 1153–1157 (2010).
23. W. S. Zaoui, H.-W. Chen, J. E. Bowers, Y. Kang, M. Morse, M. J. Paniccia, A. Pauchard, and J. C. Campbell, "Frequency response and bandwidth enhancement in Ge/Si avalanche photodiodes with over 840 GHz gain-bandwidth-product," *Opt. Express* **17**(15), 12641–12649 (2009).
24. J. S. Ng, C. H. Tan, J. P. R. David, and G. J. Rees, "A general method for estimating the duration of avalanche multiplication," *Semicond. Sci. Technol.* **17**(10), 1067–1071 (2002).

## 1. Introduction

Compared to conventional photodiodes, APDs provide avalanche gains, which can yield higher overall signal-to-noise ratios for the receiver modules, if the receivers' noise is dominated by the amplifier circuit. This is particularly important to high-speed receiver modules. Commercial telecom APDs combine an InGaAs absorption layer with an InP avalanche layer and are suitable up to 10 Gb/s. The next generation 100 and 400 GHz Ethernet systems have spurred the demand for higher bit rate APDs to meet the demands of "big data" [1]. To improve APD speed performance, very thin avalanche layers are generally required so that avalanche buildup time is minimized [2]. Very thin avalanche layers are however susceptible to band-to-band tunnelling currents, which increase exponentially with electric fields and add to the receiver's noise, through leakage currents. Thus, practical lower limits exist for the avalanche layer thickness to avoid excessive tunnelling currents.

Using bit-error-rate simulations, values for these limits were predicted for InP and  $\text{In}_{0.52}\text{Al}_{0.48}\text{As}$ , the typical avalanche layer materials in APDs for 1310 and 1550 nm wavelength receiver modules [3]. Experimental reports of the Gain-Bandwidth Product (GBP) are indeed limited to 80 - 120 GHz [4–6] and 105 - 160 GHz [7–10] for the InGaAs/InP APDs and InGaAs/ $\text{In}_{0.52}\text{Al}_{0.48}\text{As}$  APDs, as illustrated in Fig. 1. Since useful avalanche gains are typically 8 to 15, these APDs are unsuitable for operation at data rates much higher than 10 Gb/s. APDs with larger GBPs have been reported but at the expense of higher leakage currents [11]. To date an InP-based telecom APD with low dark current and GBP exceeding 300 GHz remains unavailable. Very low excess noise AlInAsSb APDs grown on GaSb substrates have been reported recently, but GBP data were not available [12].

APDs with high GBPs were also developed on non-InP substrates. An example is the InAs APDs with GBP as large as 580 GHz [13], albeit with associated higher leakage currents due to the narrow bandgap of InAs. There are also high-speed APDs using Ge and Si as the light absorption material and avalanche gain material, respectively [14, 15] or Ge only [16]. However Ge/Si APDs will most likely remain limited to 1310 nm operating wavelength, due

to weak absorption of 1550 nm light in Ge. For example, the theoretical absorption efficiency at 1550 nm wavelength for a 1  $\mu\text{m}$  thick  $\text{In}_{0.53}\text{Ga}_{0.47}\text{As}$  absorption layer is double of that for the Ge counterpart.

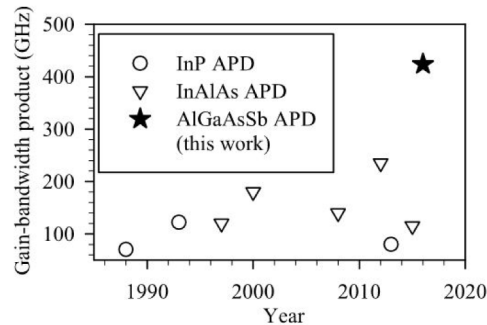


Fig. 1. Comparison of typical experimental gain-bandwidth products of APDs with InP [4–6] and InAlAs [7–10] avalanche layers.

In this work, we demonstrate a novel high speed  $\text{In}_{0.53}\text{Ga}_{0.47}\text{As}/\text{Al}_{0.85}\text{Ga}_{0.15}\text{As}_{0.56}\text{Sb}_{0.44}$  (hereafter InGaAs/AlGaAsSb) APD grown on a semi-insulating InP substrate. This builds on our earlier work that found  $\text{AlAs}_{0.56}\text{Sb}_{0.44}$  (lattice matched to InP) exhibiting very low excess noise factor [17] and low tunnelling current [18], both desirable attributes for avalanche materials. It is not entirely surprising that  $\text{AlAs}_{0.56}\text{Sb}_{0.44}$  may offer a practical lower limit for the avalanche layer since materials with large and indirect bandgaps have less significant tunnelling currents, compared to those with small and direct bandgaps. The quaternary alloy  $\text{Al}_{0.85}\text{Ga}_{0.15}\text{As}_{0.56}\text{Sb}_{0.44}$  has an indirect bandgap of 1.56 eV and exhibits insignificant tunnelling current in a thin 100 nm avalanche layer [19]. Its lower Al content will also reduce undesirable oxidization. This large bandgap, compared to those of InP (1.34 eV [20]) and InAlAs (1.45 eV [21]), should allow a thin AlGaAsSb avalanche layer be used to produce a high GBP without excessive band-to-band tunnelling current.

## 2. Experimental details

The structure was grown on a semi-insulating InP substrate by solid source molecular beam epitaxy. The p-type layers were doped with Be, whilst the n-type InGaAs top contact and  $\text{Al}_x\text{Ga}_{1-x}\text{As}_{0.56}\text{Sb}_{0.44}$  cladding layer were doped with Si and Te, respectively. All epitaxial layers were grown at 510°C, except for the  $\text{Al}_x\text{Ga}_{1-x}\text{As}_{0.56}\text{Sb}_{0.44}$  layers (growth temperature of 470 °C). The pseudoquaternary AlGaInAs bandgap grading layers were grown using digital alloys of  $\text{In}_{0.53}\text{Ga}_{0.47}\text{As}$  and  $\text{In}_{0.52}\text{Al}_{0.48}\text{As}$ . The wafer structure, a top-view photo and a cross-sectional 3-D illustration are shown in Table 1, Fig. 2(a) and Fig. 2(b), respectively. All data were obtained from APDs with diameter  $D$  of 20  $\mu\text{m}$ , unless otherwise stated.

The wafer was first annealed by rapid thermal annealing at 500 °C for 90 s to encourage activation of dopants in the wide bandgap AlGaAsSb field control layer and n cladding layer. Top illuminated mesa APDs with diameters  $D$  of 20, 120, 220 and 420  $\mu\text{m}$  were then fabricated. The mesa etching used a mixture of hydrochloric acid: hydrogen peroxide: deionized water (ratio of 1:1:5), followed by a mixture of sulphuric acid: hydrogen peroxide: deionized water (ratio of 1:8:80). InGe/Au (20/200 nm) and Au/Zn/Au (20/20/200 nm) were thermally evaporated to form top n- and bottom p- electrical contacts. For devices with  $D = 20 \mu\text{m}$ , the mesa etching reached the InP substrate. This was followed by deposition of a ~700 nm  $\text{SiN}_x$  passivation layer using a Plasma Enhanced Chemical Vapour Deposition machine, with the sample heated to 150 °C. Finally bond pads to the n- and p- contacts were formed by depositing Ti/Au (10/500 nm). The devices did not have anti-reflection coating on the top nor reflecting mirror at the bottom.

Table 1. Wafer Structure

Type	Doping density ( $\text{cm}^{-3}$ )	Thickness (nm)	Material	Function
n	$5.0 \times 10^{19}$	50	$\text{In}_{0.53}\text{Ga}_{0.47}\text{As}$	Contact
n	$3.4 \times 10^{18}$	150	$\text{Al}_{0.85}\text{Ga}_{0.15}\text{As}_{0.56}\text{Sb}_{0.44}$	Cladding
i		100	$\text{Al}_{0.85}\text{Ga}_{0.15}\text{As}_{0.56}\text{Sb}_{0.44}$	Avalanche
p	$1.15 \times 10^{18}$	47	$\text{Al}_{0.85}\text{Ga}_{0.15}\text{As}_{0.56}\text{Sb}_{0.44}$	Field-control
i	–	25	$\text{Al}_{0.85}\text{Ga}_{0.15}\text{As}_{0.56}\text{Sb}_{0.44}$	Bandgap grading
	–	25	$\text{In}_{0.52}\text{Al}_{0.48}\text{As}$	
	–	25	$\text{Al}_{0.27}\text{Ga}_{0.2}\text{In}_{0.53}\text{As}$	
	–	25	$\text{Al}_{0.13}\text{Ga}_{0.34}\text{In}_{0.53}\text{As}$	
i	–	300	$\text{In}_{0.53}\text{Ga}_{0.47}\text{As}$	Absorption
i	–	25	$\text{Al}_{0.13}\text{Ga}_{0.34}\text{In}_{0.53}\text{As}$	Bandgap grading
	–	25	$\text{Al}_{0.27}\text{Ga}_{0.2}\text{In}_{0.53}\text{As}$	
	–	25	$\text{In}_{0.52}\text{Al}_{0.48}\text{As}$	
p	$5 \times 10^{18}$	300	$\text{In}_{0.52}\text{Al}_{0.48}\text{As}$	Cladding
p	$5 \times 10^{19}$	500	$\text{In}_{0.53}\text{Ga}_{0.47}\text{As}$	Contact

Semi-insulating InP substrate

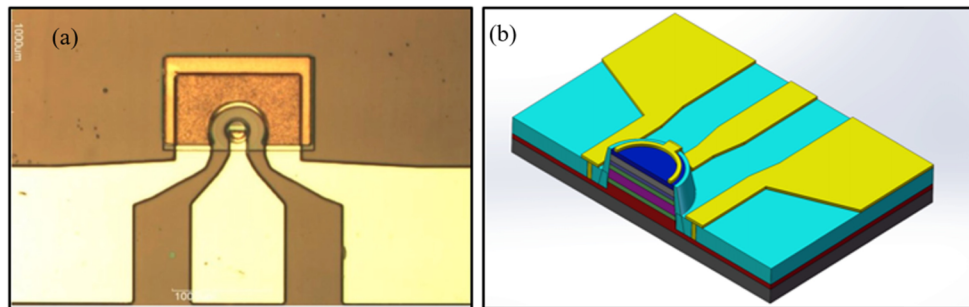


Fig. 2. (a) A top-view photo and (b) a 3-D cross-sectional illustration of the InGaAs/AlGaAsSb APD.

Current-Voltage measurements were carried out using a source-measurement-unit. For 200 K measurements, the sample was placed in a Janis ST-500 probe station. The photocurrent was measured using the phase sensitive detection technique with a combination of modulated laser light and a lock-in amplifier. Care was taken to avoid illuminating the sidewalls of the device-under-test.

Avalanche gain,  $M$ , was given by the ratio of measured responsivity to the theoretical responsivity at unity gain. Values of responsivity were given by the ratio of measured photocurrent to the optical power incident on the APD (determined using an optical power meter). For the theoretical responsivity at unity avalanche gain for our APD, we utilised a reference photodiode, which contained an InGaAs absorption layer, bandgap grading layers and cladding layers with thicknesses identical to equivalent layers in the APD. Including a 30% reflection loss at the air/semiconductor interface, the responsivity at unity gain was found to be 0.176 A/W at 1550 nm wavelength.

The on-wafer frequency response measurements were performed at the laser wavelength of either 1310 nm or 1550 nm with a 40 GHz electron-absorption modulator. The modulator was driven by a 50 GHz Agilent Network Analyser with a modulating RF power of  $-10$  dBm. The modulated laser light was delivered to the APD via a standard fibre. The system's frequency response was calibrated using a high speed photodiode with a  $-3$  dB bandwidth of 50 GHz (U2t photonics photodetector XPDV2120R). The on-wafer eye diagram measurement setup consisted of a 1550 nm laser diode, a 35 GHz  $\text{LiNbO}_3$  modulator (biased at quadrature and operating with non-return-to zero on-off keying, pseudo-random binary signal of length  $2^7-1$ ) and a digital communication analyser.

### 3. Results and discussions

Dark current-voltage characteristics of the APDs at room temperature down to 77 K are shown in Fig. 3(a). A steep increase in the dark current occurs at  $-15$  V, followed by a more gradual increase at higher bias. Dark current at biases above  $-15$  V reduces rapidly as the temperature decreases. The large decrease suggests that the dark current is not dominated by band-to-band tunnelling current, which has weak temperature dependence [22]. The total dark current can be expressed as  $I_{dark} = A\pi D + B\pi D^2/4$ , where  $A$  is the surface dark current per unit length,  $B$  is the bulk dark current per unit area, and  $D$  is the diameter of the APD. Thus total dark current density is given by  $J_{dark} = 4A/D + B$ . We found  $J_{dark}$  increases as  $D$  reduces (not shown here), indicating significant surface leakage current in these APDs. The surface leakage currents were attributed to the mesa profiles (obtained by Scanning Electron Microscopy) that are far from the ideal (vertical profiles in all orientations). These profiles resulted from differences in etch rates for the different materials (hence InAs APDs [13] are largely unaffected). Improving the mesa profile would help to reduce the surface leakage currents in the InGaAs/AlGaAsSb APDs.

Photocurrent generated using a 1550 nm laser is shown in Fig. 3(b). A sharp increase in the photocurrent occurs around  $-14.5$  V, before the rapid onset of dark current at 15 V. We interpret  $-14.5$  V as the punch-through voltage, at which the depletion region extends into the InGaAs absorption layer, increasing the collection efficiency of photo-generated carriers significantly. Using a 1550 nm laser with an optical power of  $50 \mu\text{W}$  (when unmodulated), we obtained a responsivity of  $0.98 \text{ A/W}$  at the punch through voltage, suggesting a rather large avalanche gain of 5.6. A maximum responsivity of  $5.33 \text{ A/W}$ , corresponding to  $M = 30.3$ , was obtained at  $-21$  V.

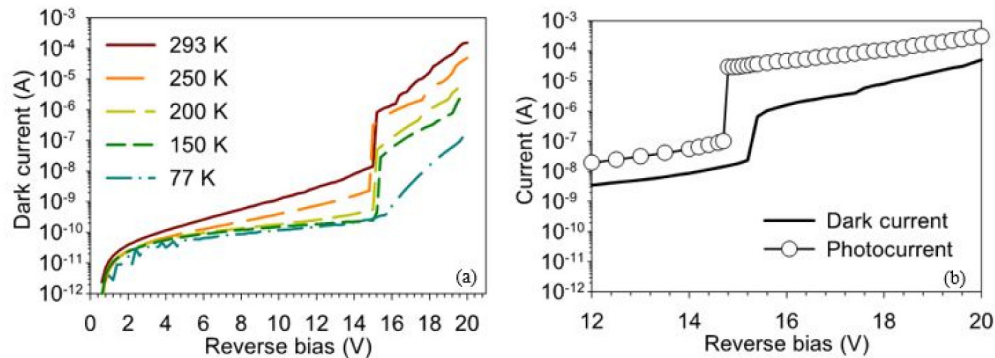


Fig. 3. Current-Voltage characteristics of  $20 \mu\text{m}$  diameter APDs. (a) Dark current at room temperature down to 77 K. (b) Room temperature dark current and photocurrent around  $-15$  V.

The frequency responses of the APD were recorded under voltages from  $-15$  to  $-21$  V, also with optical power of  $50 \mu\text{W}$  (unmodulated). Figure 4(a) shows the frequency response increasing in magnitude and widening with reverse bias. For instance the avalanche gain produces a 10 dB signal enhancement at frequencies between 3.5 and 10 GHz when the bias increases from  $-15$  to  $-21$  V. Figure 4(b) shows the  $-3$  dB bandwidth and GBP versus  $M$ . A maximum bandwidth of 14 GHz was achieved at the bias of  $-21$  V. Measurements at higher bias were limited by the presence of a high dark current. The increasing bandwidth with avalanche gain suggests that the performance of our APD is not yet limited by the avalanche gain. A maximum bandwidth of 14 GHz with a gain of 30.3 yields a GBP of 424 GHz at  $-21$  V. It is unusual to have such large GBP values without having already encountered a constant GBP limit. This may be due to increased carriers' velocities from changes in electric field profiles [23] and/or enhancement in the average speed of carriers which ionize early in their trajectories [24].

For 20  $\mu\text{m}$  diameter diodes, the RC-limited bandwidth is  $> 35$  GHz (75  $\Omega$  series resistance and 55 fF capacitance) and the transit time-limited bandwidth is  $> 70$  GHz (600 nm total depletion width and  $10^5$   $\text{ms}^{-1}$  saturated carrier velocity). Assuming equal electron and hole ionization coefficients (worst case for gain-limited bandwidth) for a 100 nm avalanche region, the gain-limited bandwidth is 16 GHz when gain is 30 (GBP  $\sim 480$  GHz). Our highest values for bandwidth and GBP (14 GHz and 424 GHz) are thus below the most stringent limit from avalanche gain.

High frequency performance of the APD was also assessed using on-wafer eye diagrams. The data measured at bias of  $-15$  V and  $-19$  V, without post RF amplifier, are shown in Fig. 5. With increased signal amplitude at  $-19$  V a clear opening of  $\sim 3$  mV can be observed.

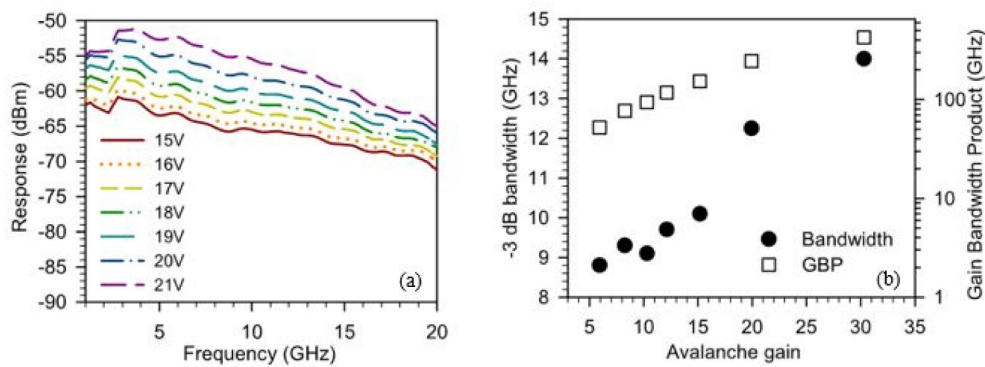


Fig. 4. High frequency performance of 20  $\mu\text{m}$  diameter APDs. (a) Response versus frequency with the APD biased at  $-15$  to  $-21$  V, in 1 V step. (b)  $-3$  dB bandwidth and GBP versus avalanche gain.

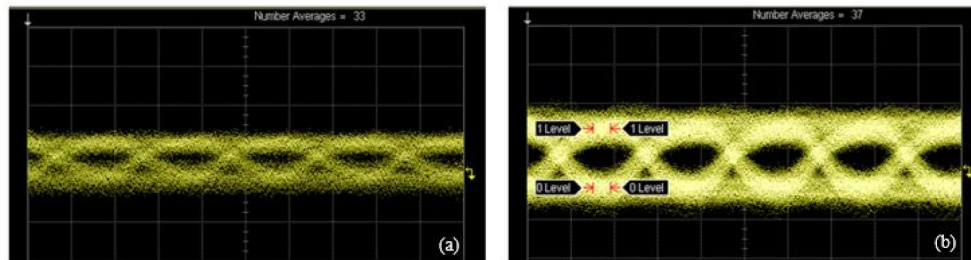


Fig. 5. 10 Gb/s eye diagram for InGaAs/AlGaAsSb SAM APD with 20  $\mu\text{m}$  diameter at bias of (a)  $-15$  V and (b)  $-19$  V. The vertical scale is 2 mV/division and the time scale is 50 ps/division.

#### 4. Conclusions

We have carried out detailed device characterization on our InGaAs/AlGaAsSb APDs. The work is the first demonstration of an APD with a high GBP over 400 GHz that is compatible to InP technology, with clear exploitation in telecom/data communication networks at 10 Gb/s or above. This is a step change in performance compared to previous reports of GBP values from 1550 nm wavelength APDs. The APD exhibits insignificant band-to-band tunnelling current, maximum responsivity of 5.33 A/W at 1550 nm, a maximum  $-3$  dB bandwidth of 14 GHz and a clear eye diagram at 10 Gb/s.

#### Funding

UK Engineering and Physical Sciences Research Council (EPSRC) (EP/K001469/1); Royal Society (University Research Fellowship for J. S. Ng).